CTOA testing of pipeline steels using MDCB specimens[1]

by Dr Robert L Amaro, Dr Jeffrey W Sowards, Elizabeth S Drexler, J David McColskey, and Christopher McCowan*

NIST, Applied Chemical and Materials Division, Boulder, CO, USA

THE CRACK-TIP-OPENING angle (CTOA) is used to rank the relative resistance to crack extension of various pipeline steels. In general, the smaller the CTOA value, the lower the resistance to crack extension. It is unclear, however, whether CTOA is a material property that is valid for all thicknesses and rates of crack growth. Historically, drop-weight tear tests (DWTT) and modified double-cantilever beam (MDCB) specimens have been used for measuring CTOA. Tests using either specimen may be conducted at quasi-static and dynamic rates. The fastest displacement rates achieved in our laboratory were near 14 m/s, resulting in crack extension rates near 30 m/s for high-toughness linepipe steels. In-service crack extensions for ductile-crack fracture can be more than 100 m/s. The failure mode at this rate is plastic collapse, and it is uncertain if correlations can be drawn between in-service failures and laboratory tests conducted on thinner material tested at slower rates. We describe the evolution of our test method using MDCB specimens from 2006 to 2012 and the direction we anticipate for future CTOA research.

THE INCREASING DEMAND for natural gas as an alternative energy source implies continued growth of gas pipeline installations and the qualification of materials in the actual pipeline network. A difficult problem to be solved for the economic and safe operation of high-pressure gas pipelines is the control of ductile-fracture propagation [1]. As a result, the accurate prediction of the resistance to fracture and ductile-fracture arrest in pressurized gas pipelines are currently important issues.

Initially, the measure of a material's fracture resistance was determined on the basis of Charpy V-notch (CVN) shelf energy, such as that used in the Battelle two-curve model [1]. Later correlations were developed between Charpy and dynamic drop-weight tear test (DWTT) data. The Battelle two-curve model worked well for many years, but when applied to modern higher-strength pipeline steels, significant errors are apparent [2–5]. Correction factors have been developed [1,4,5] for high-strength steels; however, use of these correction factors adds further uncertainty to the estimates. Thus, in parallel with the CVN- and DWTT-based fracture strategies, pipeline designers have worked on developing new measures of fracture control. Among these, crack-tip-opening angle (CTOA) is one alternative for characterizing fully plastic fracture [6-7], especially for running ductile cracks in pipes [2,7-13]. In cases where the fracture process is characterized by a large degree of stable tearing, CTOA has been recognized as a measure of the resistance of a material to fracture [6,9]. The main advantages of CTOA are that it can be directly measured from the crack-opening profile and can be related to the geometry of the fracturing pipe. However, there are difficulties in determining CTOA with a simple measurement technique that would be widely available to many material-test laboratories. In addition, the CTOA criterion can be implemented in finite-element models of the propagating-fracture process [6,9,13,14].

The literature contains a number of different specimen geometries for studying ductile-fracture propagation with the CTOA criterion, such as middle-tension specimens, M(T) [6,15,16], compact-tension specimens, C(T) [6,15,16], DWTT specimens (with methodologies based on one specimen [1,8,9,10] or two specimens [17]), three-point bend specimens, 3-PB [7,12], and modified double-cantilever beam specimens, MDCB [3,13]. Our efforts have focused on test methods using the MDCB specimen [3,13,18-20] that is promising for CTOA measurement in pipeline steel, because this specimen design allows an extended region for steady-state crack growth and for larger plastic deformation at the crack tip. This may

1. Contribution of NIST, an agency of the US government: not subject to copyright in the United States.

*Corresponding author's contact details:
tel: +1 303 497 3699
email: charpy@boulder.nist.gov

ID Number	API Designation	SMYS MPa (ksi)	O.D. mm(inch)	Thickness mm
1	N/A (~X70)	517 (75)	0.51 (20)	9.7
2	X52	359 (52)	0.51 (20)	8.0
3	Grade B	244 (35)	0.56 (22)	7.4
4	N/A (~X52)	335 (48)	0.51 (20)	7.9
5	N/A	281 (40)	0.56 (22)	7.8
6	X65	448 (65)	0.61 (24)	31.5
7	X65	448 (65)	0.51 (20)	25.0
8	X65	448 (65)	0.76 (30)	17.0
9	X100	689 (100)	1.32 (52)	20.6
10	X100	689 (100)	1.22 (48)	20.0
11	X100	689 (100)	1.22 (48)	20.0
12	X70 spiral	483 (70)	0.91 (36)	13.7

Table 1. Information on pipeline steels tested.

simulate the conditions surrounding running cracks on pipelines as they exhibit plastic regions on the order of 2.5 pipe diameters ahead of the crack tip and 0.3 diameters on each side of the crack line [10]. Moreover, the MDCB specimen can be cut directly from pipe with no subsequent flattening required, which avoids potential load-history effects due to pre-straining the material.

NIST has a history of conducting CTOA tests with the MDCB specimen. The gripping mechanism has evolved to increase constraint, methods to mark grids on the specimens have improved, and loading and recording systems were developed to conduct tests at high rates [21-31].

In this summary of our CTOA testing, data from 12 pipeline steels are presented. They are described here and referenced by ID number in the sections that follow. Table 1 summarizes the dimensions of the pipes from which all samples were extracted. The specified minimum yield strength (SMYS) and the API designations are also provided in the table. In Table 2, the chemical compositions of the steels are given, while in Table 3, the grain size and pearlite volume fraction are given for the ferrite/pearlite steels (#1 - #5).

Microstructures

The microstructures of the 12 pipeline steels tested are briefly described as follows:

- Steel #1 is a ferrite-pearlite steel with low carbon (low pearlite) content and a fine ferrite grain size. This steel represents a modern, fine-grained ferrite pipeline steel.
- Steel #2 is an API X-52 characterized by a ferrite-pearlite structure, with a significantly larger ferrite grain size than steel #1. This steel has the most pronounced banding (of pearlite) of the steels evaluated here.
- Steel #3 is an API Grade B ferrite-pearlite steel without banding.
- Steel #4 is a ferrite-pearlite steel with low banding.
- Steel #5 is a ferrite-pearlite steel without banding.
- Steel #6 is an API X-65 grade of ferrite-pearlite steel, which might be better described as ferrite-carbide, because there is very little pearlite in the microstructure. The grain size of this steel was not measured, but the ferrite grain size is similar in size to that of steel #1.
- Steel #7 is an API X-65 grade with no pearlite and a fine non-equiaxial microstructure.
- Steel #8 is an API X-65 grade with a ferrite-pearlite microstructure and heavy bands of pearlite.
- Steel #9 is an API X-100 grade: this is an experimental alloy that was used for full-scale testing.
- Steels #10 and #11 are two modern API X-100 bainitic steels.
- Steel #12 is an API X-70 spiral pipe steel, the microstructure of which is not known.

Tensile properties

The tensile properties of steels #1 to #5 were measured with flat tensile specimens (due to plate thickness), while round tensile specimens (6-mm diameter) were tested for steels #6 to #11. The flat specimens were

	#1	#2	#3	#4	#5	#6
Al						0.031
B						<0.0002
C	0.06	0.24	0.27	0.18	0.25	0.07
Co	0.006	0.025	0.007	0.014	0.025	0.003
Cr	0.02	0.024	0.029	0.021	0.019	0.12
Cu	0.11	0.038	0.015	0.054	0.046	0.12
Mn	1.46	1.03	0.36	0.52	0.97	1.48
Mo	0.025	0.016	0.007	0.009	0.017	0.003
N						
Nb	0.054	0.007	0.005	0.005	0.007	0.04
Ni	0.10	0.064	0.021	0.021	0.066	0.17
P	0.01	0.016	0.005	0.026	0.013	0.008
S	<0.01	0.013	0.015	0.010	0.012	0.004
Si	0.28	0.057	0.009	0.043	0.061	0.094
Ti						0.03
V	0.045	0.002	0.003		0.002	0.04

	#7	#8	#9	#10	#11	#12
Al	0.030	0.039		0.025	0.012	0.039
B	<0.0002	0.0002			<0.0001	0.0003
C	0.07	0.08	0.07	0.084	0.064	0.04
Co	0.002	0.001			0.003	
Cr	0.13	0.03		0.021	0.023	0.07
Cu	0.10	0.09	0.30	0.286	0.28	0.31
Mn	1.59	1.56	1.90	2.092	1.87	1.56
Mo	0.003	0.006	0.15	0.127	0.23	0.20
N				0.005	0.003	0.008
Nb	0.03	0.04		0.041	0.017	0.069
Ni	0.14	0.21	0.50	0.501	0.47	0.11
P	0.009	0.011	0.008	0.10	0.009	0.010
S	0.004	0.003	0.0005	0.002	<0.001	0.009
Si	0.092	0.325	0.10	0.108	0.099	0.24
Ti	0.02	<0.01		0.007	0.17	0.013
V	0.04	0.04		0.006	0.002	0.003

Table 2. Chemical composition of the pipeline steels tested, by mass. Column numbers give identification number for the steel, as defined in Table 1.

Steel #	1	2	3	4	5
Ferritic grain size (μm)	6.5	11.8	10.8	N/A	22.2
Pearlite volume fraction (%)	5	37.1	25.3	37.9	17.1

Table 3. Measurements of the grain size and ferrite fraction for the ferrite/pearlite steels.

Steel #	Orientation	E (GPa)	$\sigma_{0.2}$ (MPa)	σ_{UTS} (MPa)	$\sigma_{0.2}/\sigma_{UTS}$	e_u (%)	e_f (%)	e_u/e_f
1	L	211*	517	611	0.846	6.7%	35.0%	0.19
	T	N/A	543	606	0.896	8.0%	27.4%	0.29
2	L	211*	360	556	0.647	12.3%	32.7%	0.38
	T	N/A	448	576	0.777	11.1%	25.6%	0.43
3	L	212*	244	451	0.541	19.6%	37.8%	0.52
	T	N/A	255	459	0.555	18.8%	38.0%	0.49
4	L	210*	335	535	0.626	12.9%	34.9%	0.37
	T	N/A	428	560	0.764	10.5%	22.0%	0.48
5	L	214	265	454	0.583	16.0%	38.0%	0.42
	T	NA	248	453	0.547	19.5%	35.0%	0.56
6	L	201	460	534	0.870	8.2%	24.7%	0.33
	T	218	497	560	0.890	7.7%	15.9%	0.48
7	L	NA	502	570	0.880	6.8%	25.7%	0.26
	T	N/A	511	577	0.885	7.2%	20.9%	0.34
8	L	217	522	618	0.844	10.1%	27.3%	0.37
	T	N/A	576	644	0.894	6.9%	24.8%	0.28
9	L	N/A	694	801	0.910	4.6%	20.3%	0.23
	T	N/A	797	828	0.966	4.1%	19.3%	0.21
10	L	192	722	855	0.844	4.6%	17.8%	0.26
	T	213	912	916	0.995	2.6%	18.0%	0.14
11	L	198	729	838	0.869	5.8%	20.5%	0.28
	T	207	833	868	0.989	4.7%	17.5%	0.27
12	T	NA	576	650	0.940	NA	NA	NA
*Average determined from dynamic elastic modulus test								

*Table 4. Tensile properties of the materials. (Note: * = average determined from dynamic-elastic-modulus test.)*

6 mm wide. Full-thickness specimens (Table 1) were tested for the longitudinal orientation, and typically 3-mm thick specimens were tested for the transverse orientation. All specimens had a gauge length of 25.4 mm. Experiments were performed either in a screw-driven tensile testing machine of 100-kN capacity, or a closed-loop servo-hydraulic machine of 100-kN capacity. Tests were conducted in displacement control at rates of 0.25 mm/min for the flat specimens and 0.1 mm/min for the round specimens.

The measured mechanical properties of the steels are given in Table 4, where E is the Young's modulus, $\sigma_{0.2}$ the yield stress, σ_{UTS} the ultimate strength, e_u the uniform elongation, and e_f the fracture elongation.

In addition to the standard properties, the ratios of $\sigma_{0.2}/\sigma_{UTS}$ (stress ratio) and e_u/e_f (strain ratio) are also given in Table 4. These two parameters indicate the strain-hardening potential of the steel. As shown in Fig.1, the stress ratio increases as the strain ratio decreases.

CTOA test matrix

CTOA tests were conducted on X-52, X-65, X-70, and X-100 pipeline steels and other pipeline grades not identified with an API designation (Table 1). The tests were conducted by tensile loading MDCB specimens at actuator rates ranging from 0.002 to 14,000 mm/s. The 8,000 and 14,000-mm/s displacement rates were attained with a disc spring set-up [22]. Early tests were quasi-static, and later a series of tests were conducted on X-65 (#6) and X-100 (#9) with changing actuator rates. High-rate tests were also conducted on two additional X-100 steels (#10 and #11), and also on an X-70 steel (#12).

CTOA test specimen

A modified double-cantilever beam (MDCB) specimen (Fig.2) was used to conduct the CTOA test. The specimen exhibits the following characteristics:

- It can be cut directly from a pipe, without flattening;
- The width and thickness are limited by pipe curvature and wall thickness;
- The long ligament in the gauge section allows for the CTOA to be measured multiple times and averaged;
- High constraint in the test section is promoted by two thicker loading arms;
- The test section does not restrain the transition to slant mode shear fracture;
- The test section is flat near the crack tip for ease of CTOA measurement.

The test specimens were cut with the notch direction along the axis of the pipe. The thickness of the curved plate was reduced by machining to obtain a flat plate, which eliminated the probable residual plastic strains that would be caused by flatting the plate by use of a straightening procedure.

The specimens were fatigue pre-cracked following the ASTM standard procedure for conducting crack-tip-opening displacement (CTOD) tests [32]. The pre-cracking loads were selected to ensure that the ratio of stress intensity factor range to the Young's modulus ($\Delta K/E$) remained below 0.005 mm^{-2}. All specimens were fatigue pre-cracked at a ratio of R = 0.1 [13], to a crack-to-width ratio of a_0/W = 0.3 to 0.5 [with a specimen width, W, equal to 182 mm, and a_0 equal to the machined notch length (60 mm) plus the initial fatigue pre-crack length (approx. 10 mm)].

Methods and procedures

Two apparatuses were used for CTOA testing, a 'quasi-static' set-up and a dynamic set-up.

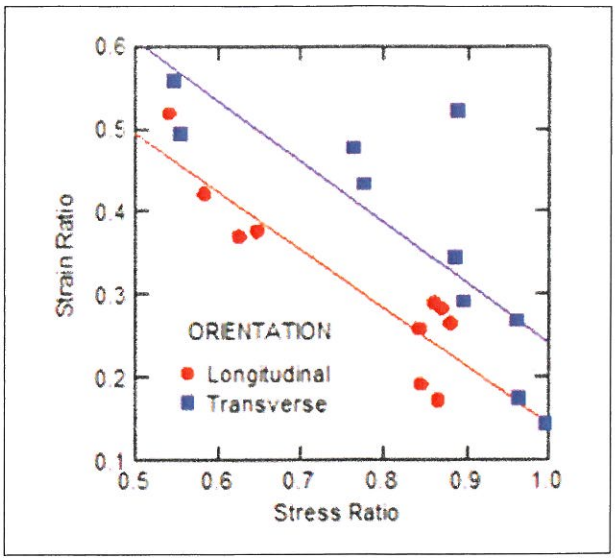

Fig. 1. Strain ratio versus stress ratio.

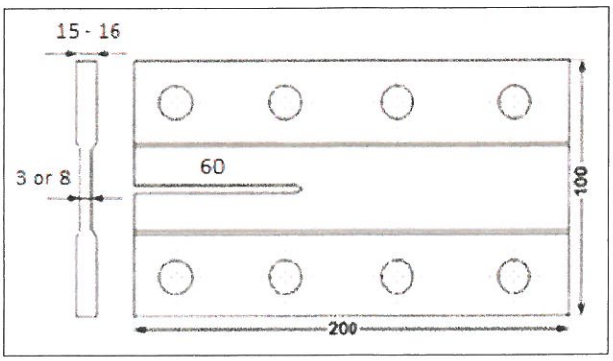

Fig.2. CTOA specimen, with dimensions in millimetres.

Quasi-static apparatus

For quasi-static testing (0.002 to 3 mm/s), a 250-kN uniaxial servo-hydraulic test machine was used. Tests were conducted in displacement control. As shown in Fig.3a, the load line ran through the centreline of the first pair of holes in the specimen. A digital camera and frame-capture software/hardware were used to capture images. The camera was mounted on an XYZ stage, which provided a stable platform to follow the crack tip. The image acquisition was controlled by a personal computer with image-analysis software: the captured images had a size of 2048 pixels × 1536 pixels, which resulted in a resolution of about 32 pixel/mm. Images were acquired and stored, along with time, load, and displacement data as the crack propagated across the specimen. Tests were stopped at 80 mm of crack extension beyond the machined notch tip. Details of the set-up have been reported previously [21].

Dynamic apparatus

Tests with actuator rates of 3, 30, and 300 mm/s were performed on a 500-kN uniaxial servo-hydraulic test machine shown in Fig.3b [22]. As with the quasi-static

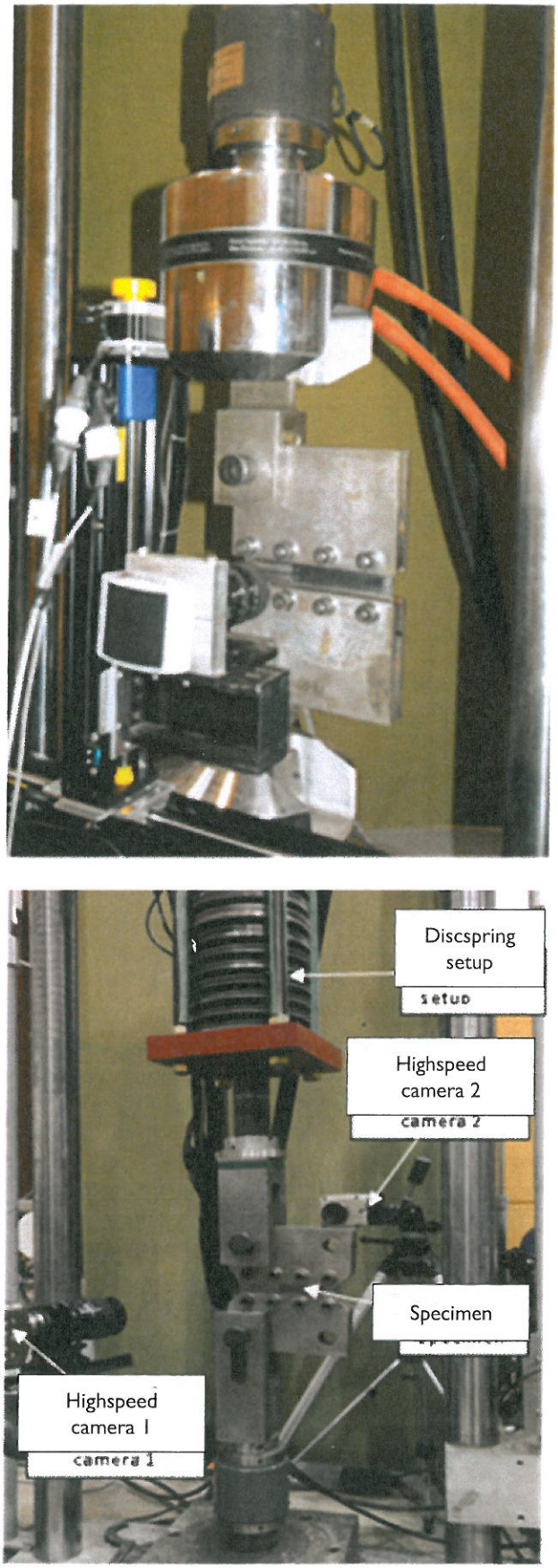

Fig.3. Set-ups for (a - top) 'static' set-up with camera on a motion-control XYZ stage, and (b - bottom) dynamic set-up with high-speed cameras and springs.

tests, the load line was located at the centreline of the first pair of holes in the specimen. The machine was adapted with large-capacity servo-valves to accomplish rapid loading. For actuator rates greater than 300 mm/s, the 500-kN uniaxial test frame was configured with a set of disc springs; the potential energies stored in these springs for the X-65 and X-100 tests were 5.6 kJ and 7.5 kJ, respectively [22]. Higher crack velocities were obtained by further increasing the stored energy with the use of sacrificial links[1], which were made of aluminium alloy 7075-T6. In this configuration, grip-displacement rates up to 14 m/s were attained.

Data processing

Once images were captured, the CTOAs were measured using data within the distance from the crack-tip ranges prescribed by the ISO draft standard [35] and the ASTM standard [36]. Within these ranges on the samples, we used the following four approaches to measure the CTOA [23]:

- Method 1 used an algorithm that located the crack tip in the data, and then selected pairs of points along the crack profile at prescribed distances from the tip to calculate CTOA. The crack tip was always included in this calculation of the CTOA.
- Method 2 used data-point pairs that were within the range 0.1 mm to 0.2 mm behind the crack tip to fit lines within this region (Fig.5a). This method never included the crack tip.
- Method 3 used data points marking the upper and lower grid lines to fit lines for CTOA calculation. Each line was fitted with 2 to 10 points, located within the increment 0.5 to 1.5 mm from the crack tip (Fig.4b).
- Method 4 used all of the profile data in the interval 0.5 to 1.5 mm to define the two best-fit lines associated with the upper and lower crack-tip profiles to calculate the CTOA. In this case, typically 100 to 200 data points were used for each line fit (Fig.4b).

The software required the operator to trace the profile of the crack tip, and mark data points along the closest set of upper and lower grid lines, as shown in Fig.4. The CTOA values for each method were then calculated from the collected images from each specimen, and an average CTOA for each method was determined.

1 Sacrificial links were inserted into the load line and loaded to compress the springs. The links were calculated to fail at the load required to full compress the springs, which resulted in abruptly releasing the stored energy onto the CTOA specimen.

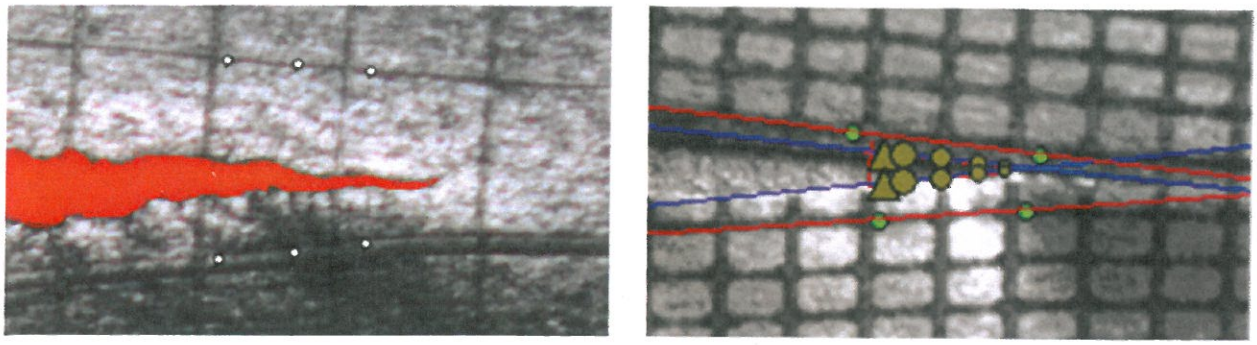

Fig.4. Showing (a - left) crack edge traced by the operator and points marked on the gridlines adjacent to the crack, and (b - right) two sets of lines fitted with grid points and crack trace respectively (grid = 1 mm x 0.5 mm).

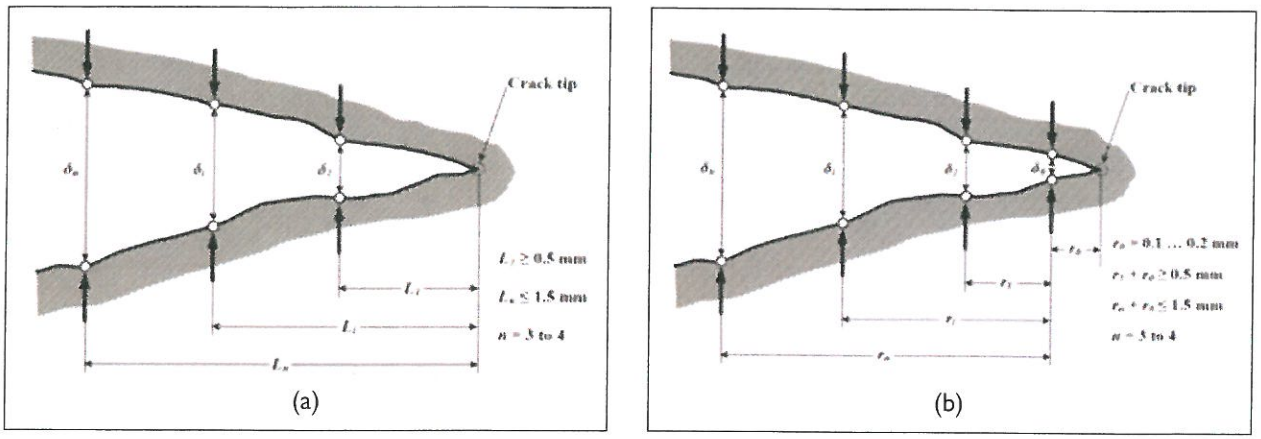

Fig.5. (a) Method 1 and (b) Method 2 for determining the CTOA. For both Methods, n was set equal to 3, $L_1 = r_1 + r_0 = 0.5$ mm, $L_2 = r_2 + r_0 = 1$ mm, and $L_3 = r_3 + r_0 = 1.5$ mm (r_0 was set to 0.15 mm).

Results and discussion

Steady-state region

CTOA values reached a constant at crack lengths ranging from about 3 to 5.2 mm, which is 1 to 1.8 times the specimen thickness. This result is consistent with those observed by Mannucci *et al.* [9], Shterenlikht *et al.* [18], and Hashemi *et* al. [3,19,20].

Comparison of CTOA algorithms

For methods that measure CTOA directly on the fracture surface (Methods 1, 2, and 4) the scatter in the CTOA decreased with an increased measurement basis (Fig.5). For example, increase in the measurement basis r reduced the standard deviation of the CTOA data from 2.11° to 0.97° for steel #1, and from 6.57° to 2.30° for steel #3. For method 1, increase in L decreased the standard deviation of CTOA measurement from 1.52° to 0.90° for steel #1, and from 1.35° to 0.76° for steel #3. This result is attributed to factors such as: the difficulty of identifying the exact location of crack edges and the crack tip; the local deformations in regions adjacent to the apparent crack tip; and the effect associated with the longer line segments. Typically, the crack edges appear to be irregular, which is a natural result of the ductile-fracture mechanism, and when all the profile data (0.5 to 1.5 mm interval) are used to fit lines and calculate CTOA for Method 4, the result compares well with the average CTOA calculated for Method 2, as expected.

Method 1 had the highest scatter in CTOA. Of the five ferrite-pearlite steels tested, only steel #1 had a standard deviation less than 1°; for the other steels, the standard deviations were between 2.2° and 4.1°. Method 1 also resulted in the highest average CTOA value for the steels. For steel #2, for example, the average CTOA value by Method 1 was 5.8° higher than that by Method 2. Method 1 depends on accurately locating the apparent crack tip, and is the most sensitive method for local deformations as well as operator judgment.

Method 2 had standard deviations in CTOA measurements between 0.7° and 0.81°, and the CTOA values consistently agreed with Method 3 more than with Method 1. Method 3 had the smallest standard deviation in CTOA values (0.46° and 0.64°). Method 4 tends to track well with Method 2 results.

More discussions of selecting a proper measurement basis L or r were given by Heerens *et al.* [36]. It can be expected that an increase of L or r may give rise to size and geometric effects. In our analysis, L or r values

Steel #	Stable CTOA (o)*	Standard deviation (o)	Cross head mm/s	Crack velocity (mm/s)
1	11.7	2.04	0.05	0.22
2	9.1	1.71	0.05	0.26
3	9.8	1.39	0.05	0.20
4	10.0	2.00	0.05	0.28
5	9.51		0.05	0.22
6	11.4		0.02	NA
7	9.9		NA	
8	NA		0.002	
9	8.6	1.42	NA	NA
10	7.8	1.9	0.02	
11	8.2	2.3	0.02	
12	11.9	1.3	0.02	NA
6-X65	11.7	1.2	0.002	0.004
6-X65	11.4	1.2	0.02	0.044
6-X65	10.5	1.0	0.2	0.5
6-X65	11.6	2.2	5	9.2±0.6
6-X65	11.0	2.4	30	45.5±1.5
6-X65	11.2	1.1	300	594±8
6-X65	11.3	1.7	8000	6500±600
9-X100	8.6	1.1	0.002	0.008
9-X100	8.3	1.8	0.02	0.088
9-X100	9.3	1.1	0.2	0.66
9-X100	9.4	1.0	3	6.7±0.7
9-X100	8.1	1.0	300	762±35
9-X100	8.8	1.6	30	118±3
9-X100	8.6	1.1	8000	7250±605
9-X100	9.8		7500	5500
10-X100	7.3	2.3	10000	13000
10-X100	10.6	5.3	20000	29000
11-X100	8.1		2900	
11-X100	8.9	2.5	8000	7000
11-X100	9.3	3.2	20000	20000
12-X70	10.2	1.8	NA	5467

Table 5. The CTOA values (Method 4) calculated for the steels at various testing rates.

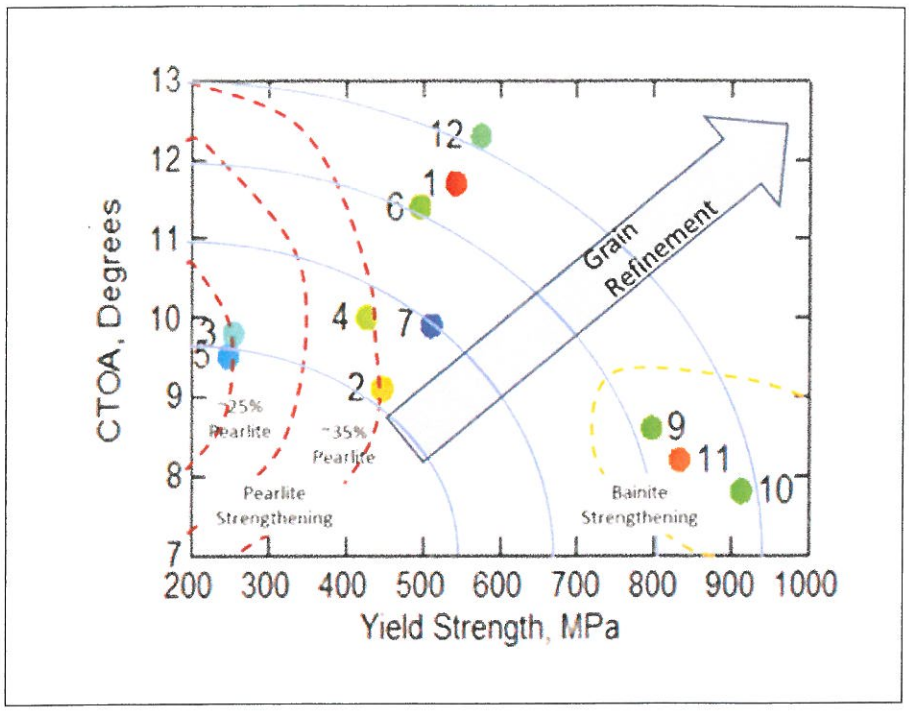

Fig.6. Ranking of steels by CTOA results.

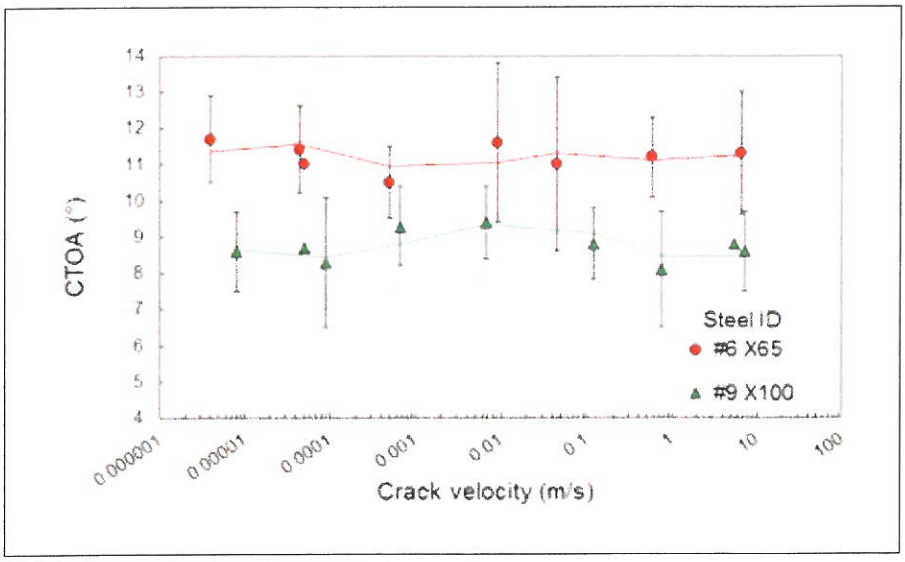

Fig.7. CTOA versus crack velocity for steel #6 (X-65) and steel #9 (X-100).

within the range from 0.5 to 1.5 mm were chosen to calculate CTOA data. This is a reasonable compromise between the demands for minimizing scatter and possible size effects in calculating CTOA for pipeline steels.

CTOA ranking of the pipeline steels tested

The results for the 12 steels are summarized in Table 5 and plotted in Fig.6, where all CTOA values were determined with Method 4 and averaged multiple specimen results. In Fig.6 the baintic steels (#9, #10, #11) have the lowest CTOA values and the highest strengths. For the ferrite-pearlite steels, we see that increasing strength by increasing the volume fraction of pearlite did not result in lowering the CTOA (#3 and #5 compared with #2 and #4). Not unexpectedly, reducing the grain size for strengthening (#1) resulted in significant increase in CTOA, as compared with steels with larger grain size but higher ferrite content at similar strength levels (#1 and #6 compared with #2 and #4). These data raise the question whether fine-grained ferritic steels with higher pearlite contents (or another strengthening addition) can provide an improvement in the strength to CTOA ratio.

Influence of loading rate on CTOA

Actuator displacement rates covering nearly seven orders of magnitude - from 0.002 mm/s to approximate 8,000 mm/s - are shown in Fig.7 for the X-65 (#6) and X-100 (#9) steels [22 and 24]. The average crack-growth velocities for the test matrix are given in Table 5.

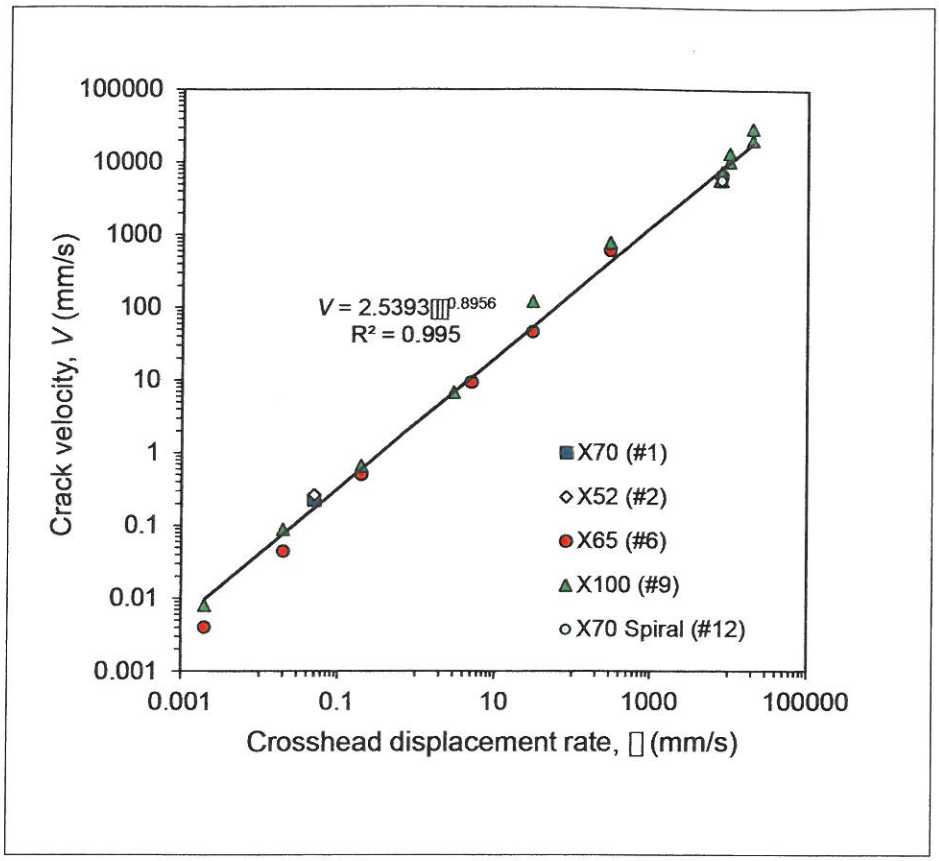

Fig.8. Crack velocity vs displacement rate.

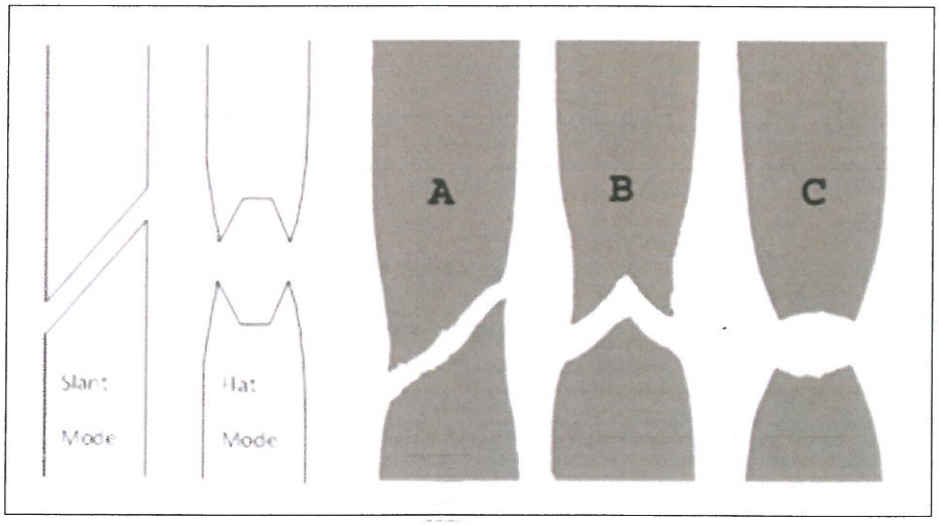

Fig.9. Idealized slant and flat fracture-mode morphologies are illustrated on the left, and traces of actual fractures are shown on the right: (A) full slant; (B) double slant; and (C) flat.

As shown in Fig.7, the CTOA results indicate that the X-65 steel (#6) consistently had a higher resistance to cracking than the X-100 steel (#9). The CTOA for the X-65 is typically more than 2° higher than the CTOA for the X-100 throughout the range of rates evaluated. Neither steel showed a trend for CTOA with actuator or crack velocity. Additional data for X-100 steels #10 and #11 provide data at rates up to 29 m/s (Table 5), and the CTOA values range from 7.3° to 8.2° with no clear trend with velocity. The X-70 steel at higher velocity (#12) had a CTOA of 10.2, and an increased crack velocity did not result in decreased CTOA.

Given that the measured CTOA values are independent of the crack-tip velocities, material-specific correlations were sought between test variables (load, displacement, displacement rate) and the measured crack-tip velocity. Not surprisingly, as shown in Fig8, the displacement rate correlates extremely well with the measured crack-tip velocity. However, for the same actuator rates, the X-65 specimens typically had a slightly lower crack velocity than the X-100 specimens, which indicates that the X-65 exhibits higher resistance to crack growth than does the X-100. It is surprising, however, that the correlation was found to be so valid for all

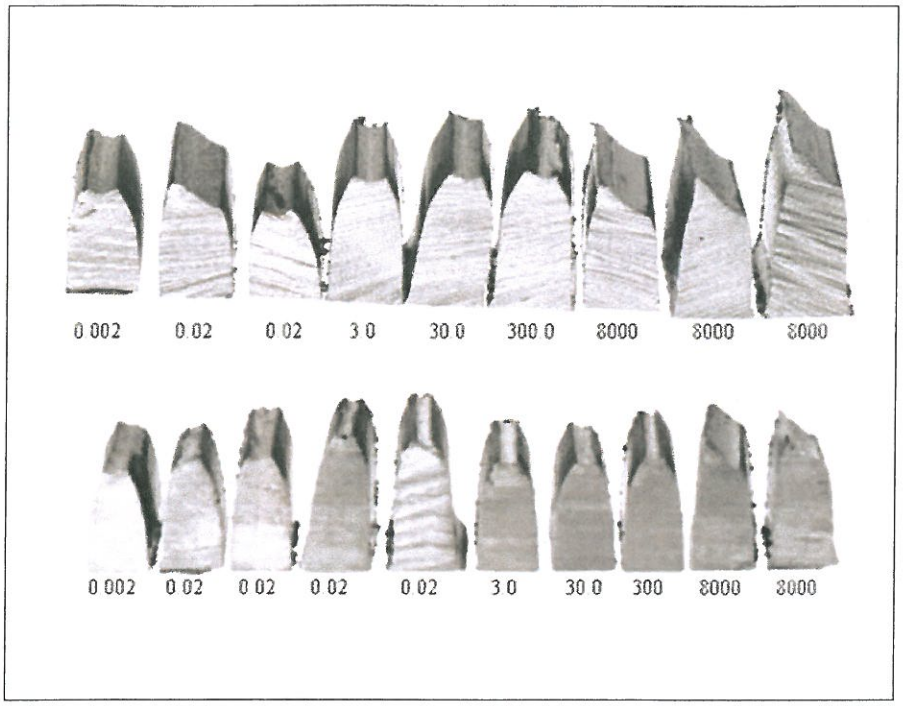

Fig.10. Cross sections of CTOD specimens of X-100 (top) and X-65 (bottom). From left to right the crosshead displacement rates applied to these specimens range between 0.002 mm/s and 8,000 mm/s. The thickness at the bottom edge of the cross sections is approximately 8 mm.

materials tested. One may infer from Fig.8 that the crack-tip velocity is primarily a function of the far-field loading rate, for the materials and loading rates tested here.

Macroscopic fracture modes

The macroscopic failure mode for pipes and CTOA specimens is often described as either a flat or a slant fracture mode (Fig.9). However, mixed-mode (flat and slant) fracture morphologies are observed for both field fractures and laboratory fractures. The range of fracture modes observed in our studies for 8-mm thick MDCB specimens is shown Fig.10: the basic slant fracture occurs on a single macroscopic shear plane through the thickness of the sample, but double-slant fractures and mixed-mode fractures are not uncommon.

Flat and mixed modes were the typical fracture modes for CTOA specimens tested at crosshead displacement rates of 300 mm/s and less (Fig.10), while at rates near 8,000 mm/s, slant fractures were typically observed. This is in agreement with fracture modes observed for full-scale, high-rate tests of the X-100. However, the fracture surface features can differ significantly, so it is useful to look a bit closer to determine whether the fracture mechanisms for laboratory fractures are representative of field fractures.

Both slant and flat fracture modes have significant areas of their fracture surfaces on angles near 45° to the applied loading. The fracture-surface features on these two types of shear-oriented surface, however, indicate that they are formed by different mechanisms. For flat fracture, the characteristic features of the CTOA specimens have much in common with the morphology-associated uniaxial tensile failures of ductile steels; however, in the case of the CTOA specimens, the morphology is cup-cup rather than cup-cone. The shear-oriented regions associated with the cup-cup fractures are formed by plastic flow that results in fractures with a knife-edge morphology. An important point associated with this observation is that the CTOA angle measured on the outside surface of a specimen in a flat-fracture mode is the angle formed between the two knife-edges as final fracture occurs. This is not an angle formed by the interior fracture planes; it is more like a plastic hinge. This is not the case for the slant-fracture mode, for which the fracture planes intersect the outside surface of the specimen.

Details of the fracture modes

Considering details for the fracture modes (Figs 11 and 12), flat fracture initiates in the centre of the specimen thickness on a plane perpendicular to the applied tensile force and grows to form an internal void. As this void grows, it effectively divides the specimen thickness into two thinner thicknesses, with lower constraint. These two thinner plates deform on shear planes until they thin down and fail in a knife-edge morphology. The ductile dimples on these thinned shear planes are characteristically elongated along the primary loading direction. But, unlike the case for cup-cone shear rupture, ductile dimples on the knife-edge cup-cup fracture surfaces do not have 'mating' dimples on the opposing fracture surface characteristic of shear failure and void sheet coalescence.

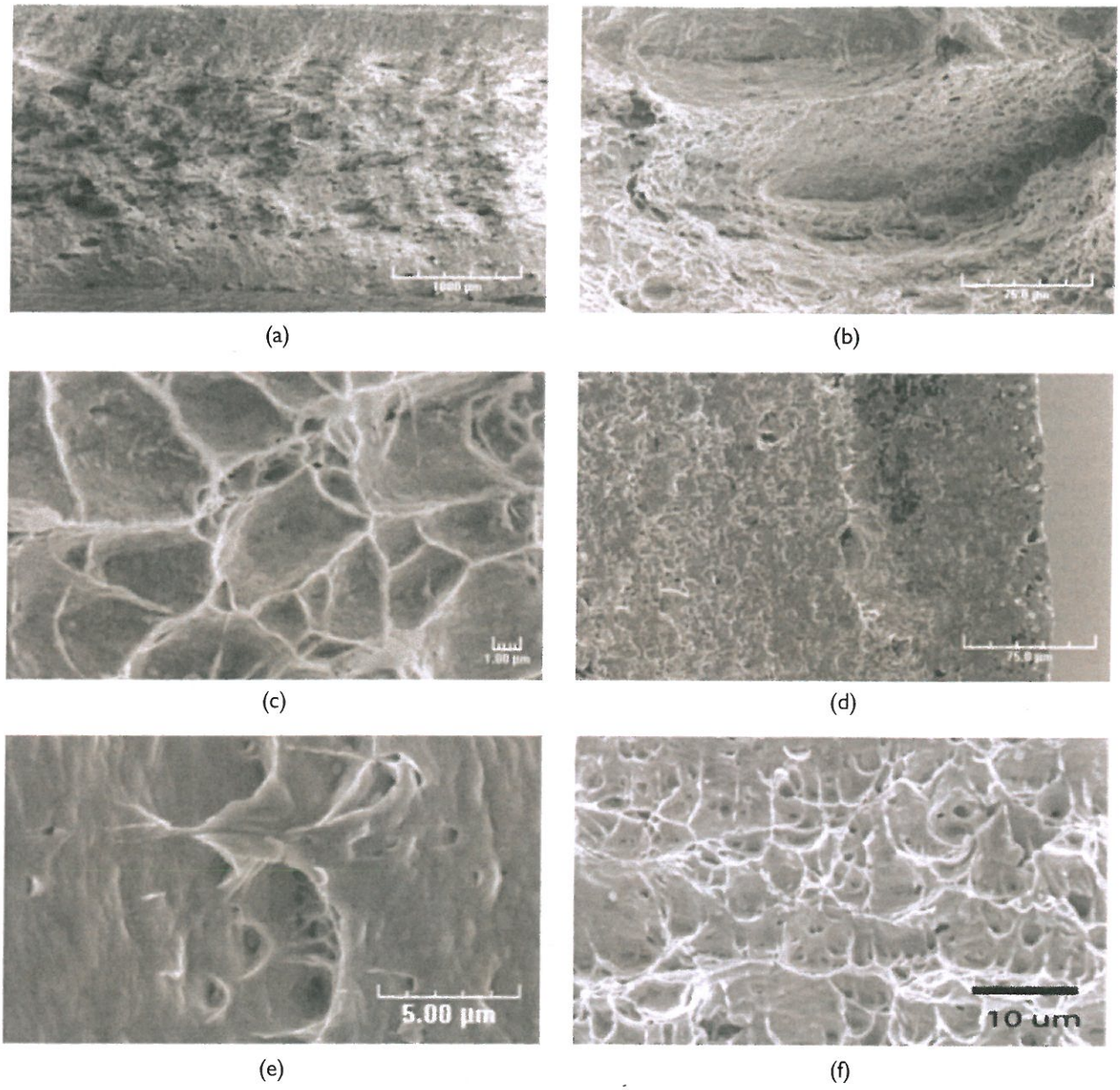

Fig. 11. Fracture-surface features associated with flat fracture. The overview (a) shows the 'flat' central portion of an X-65 fracture, bounded at both surfaces by shear regions. The central region (b and c) is a mixture of large ductile dimples, elongated in the direction of crack growth (and plate rolling), surrounded by smaller equiaxial dimples. The knife-edge final-fracture region has a shear-fracture region for a distance of about 100 µm into the specimen (d) on which shear dimples are apparent (e). There is a gradient in texture on the surface of the final fracture, with a smoother shear dimple surface near the outside edge of the specimen (e), and a more textured equiaxial dimple surface toward the centre of the specimen (f).

Due to the extensive plastic flow associated with formation of the knife-edge regions for the flat-fracture morphology, the surface roughness of these regions is smooth. As shown in Fig.11d, the surface texture near the outside surface is smooth, and this region becomes smoother and extends into the specimen further with increased testing rate. This trend is evident for both the X-65 and the X-100 steels tested, and is noticeable with the unaided eye (due to the increased light reflection for the smoother surfaces). So, flat-fracture morphologies like these like these might be interpreted to some extent to determine whether fracture occurred dynamically or not, and may give some guidance on the relative rate of fracture. These results also point out that a model of ductile fracture in pipeline steels should take into consideration the true failure mode of the steel.

A full-slant fracture mode results in the fracture surface on a single plane, tilted at an angle of 45° to the primary stress on the CTOA specimen. Details of the fracture features on these slant planes differ from those

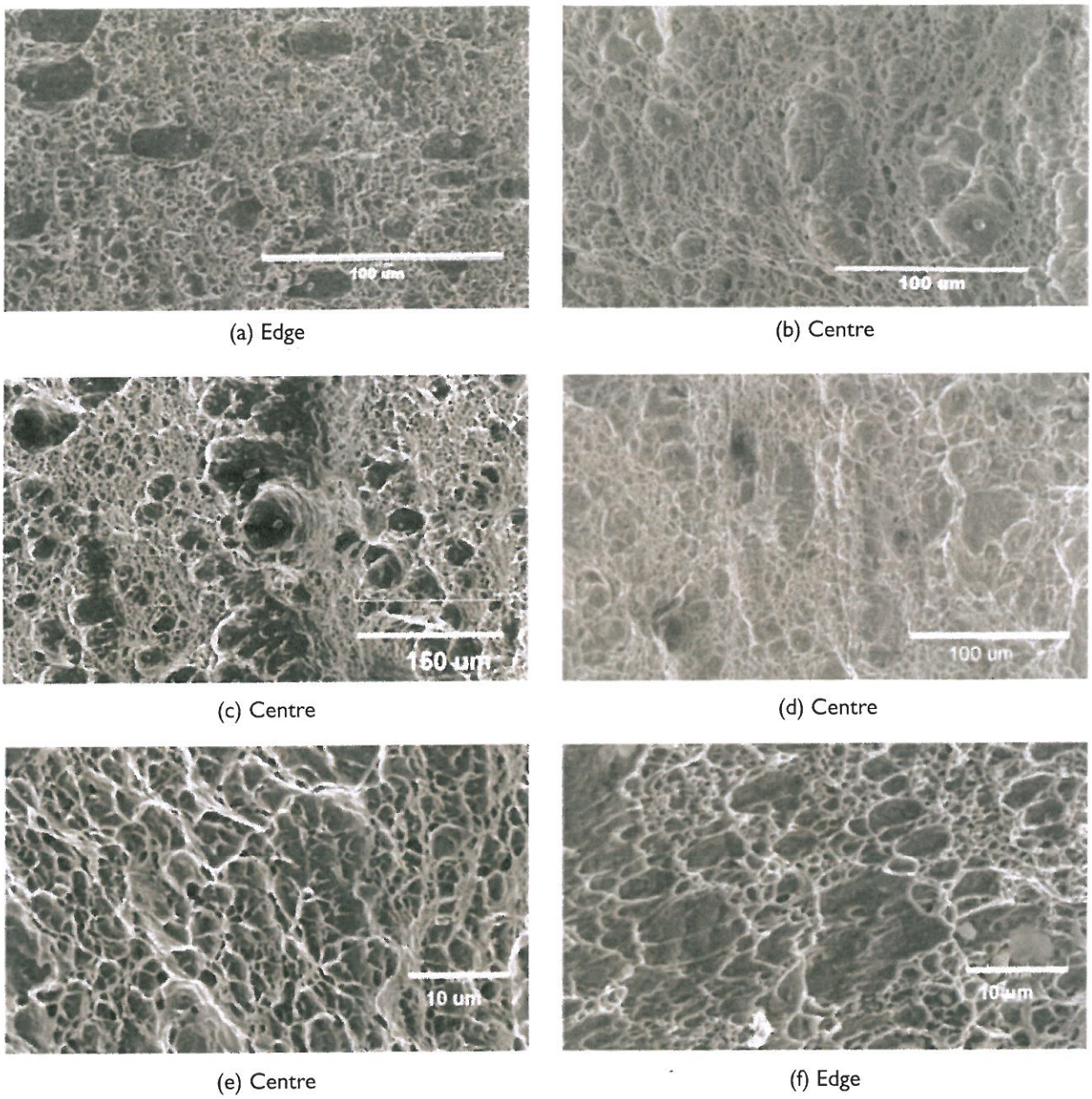

Fig.12. Details of a slant-fracture mode from an X-100 CTOA specimen showing ductile dimple morphologies: (a) region very near the outside surface of specimen, (b, c, d, e) regions through the thickness, not near the final fracture regions, (f) higher magnification of a region very close to the final fracture of the knife-edge showing shear dimples.

for both cup-cup planes, formed with the flat-fracture morphology, and shear planes formed by cup-cone failure modes (Fig.12). The ductile dimple morphology over most of the slant surface is indicative of the ductile rupture typically observed on the interior 'flat' portion of the fracture that is normal to the applied load, rather than the rupture on the shear lips of the tensile specimen. Elongated shear dimples are found only very near the outside edge of the shear planes on CTOA specimens. Across most of the slant failure, dimples are typically equiaxial and have full rims. If they are elongated, the elongation is in the direction of crack growth, as is the case for the central region of flat failure modes. This indicates that mode-I loading is the primary influence. In general, evidence of shear dimple failure (mode III) is limited to regions very near the outside surface of the specimen.

Crack-front shape

The 'crack tip' measured at the outside surface of the specimen in the CTOA test is not the tip of the crack in the interior of the specimen. For example, in Fig.13 the tip of the crack front is about 1.5 mm ahead of the intersection of the crack front with the surface of the specimen.

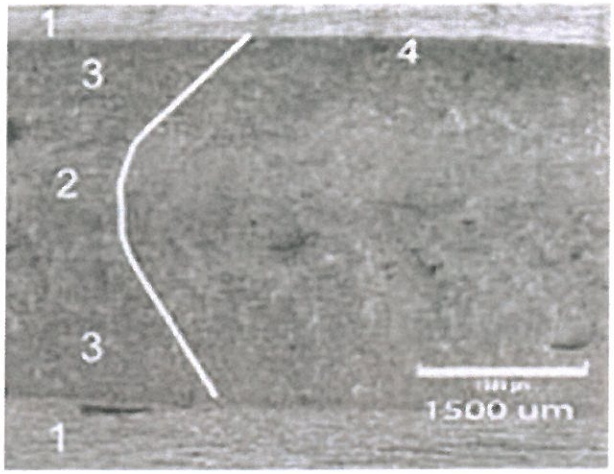

Fig.13. Crack-front trace as observed by markings on the fracture surface of a CTOA specimen. The regions of the specimen are (1) the outside surface, (2) the 'flat' portion of the fracture, (3) the 'knife-edged' portion of the surface, and (4) the final fracture region.

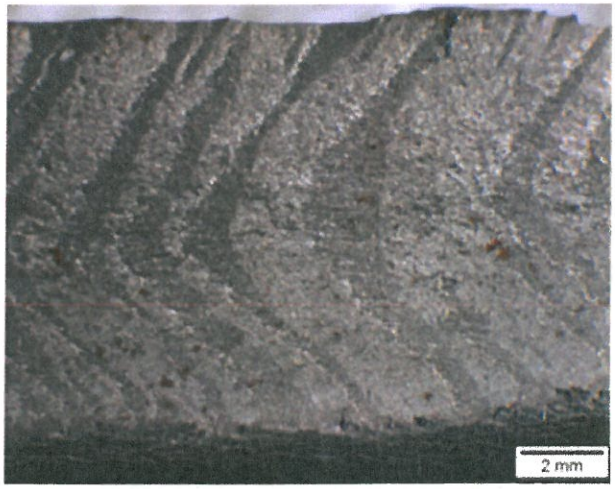

Fig.14. Intermittent bands of fast and slow ductile fracture.

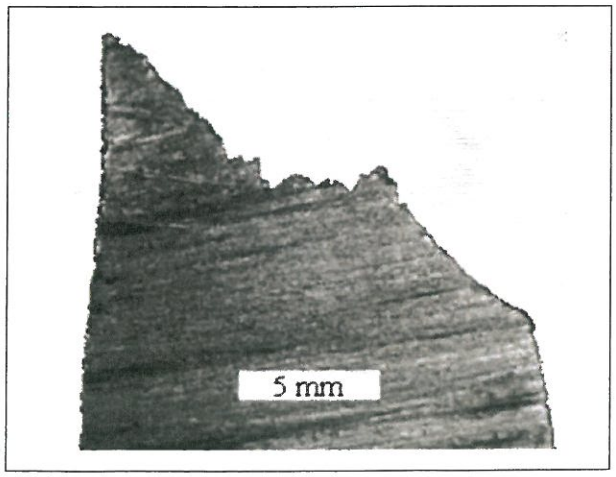

Fig.15. Cross section of an X-100 steel (#9) fractured in a full-scale test. Profiles of the fracture vary with position along the length of the fractured pipe. Some regions have flat regions joined to the outside by a slant fracture. Other regions show a full slant fracture mode.

The extent of crack-tip tunnelling varied on test specimens from about 1.5 mm to 8 mm, and the shape of the crack fronts varied from a gentle curve to an arrowhead-like shape. Occasionally crack fronts with irregular features were observed, and crack-front markings were not clear on all fracture surfaces.

Castings of CTOA specimens were made under loading to evaluate the 3D shapes of voids formed by tunnelling cracks in CTOA test specimens[1]. In the case of 'flat' fractures, the casting shapes indicate that the 'flat' fracture surfaces in the centre of the specimen thickness formed an interior CTOA of 9.2° (X-100), which compares reasonably well with the CTOA measured on the surface of the X-100 specimens. Castings also showed that the final fracture planes (knife-edge planes) on the X-100 samples were typically 45° to 50°.

Intermittent crack growth

Intermittent crack growth was sometimes observed for the X-100 specimens tested at quasi-static rates. Dark and light bands on the fracture surface mark this behaviour, as shown in Fig.14. In general, the leading edge of the crack front is coincident with the centreline of the plate (which is not always in the middle of the CTOA specimen), and intermittent crack growth does not always occur on both sides of the centreline.

Details on the fracture surface in the banded regions show regions that resemble stair steps of quasi-ductile fast fracture followed by ductile re-blunting regions [27]. The appearance of the quasi-ductile regions is similar to the details on the surfaces of secondary cracking (splits) in the burst test fractures for this X-100 steel. Since the 'riser' sections of the stair step would have the same orientation as secondary cracking, this is not too surprising. In the 'tread' orientation, ductile dimpling is apparent and indicates more ductility for this orientation. These banded regions are observed in the higher-strength materials during CTOA testing for X-80 [37] and X-100 [27, 37]. The lower-strength grades (X-65 and X-70) did not exhibit banding. Both reports suggested that the higher-strength grades may exhibit the contrasting bands due to alternating regions of quasi-cleavage and ductile fracture. Quasi-cleavage regions are likely associated with brittle microstructural constituents associated with rolling and segregation during production of higher-strength pipes.

Comparison to full-scale, high-rate test

The example shown (Fig.15) for the X-100 steel that failed in a full-scale burst test has two slant-fracture regions separated by a region of flat fracture. This is

1 Castings were made with a polysiloxane precision-impression material, a material used for dental casting. The material was injected into the crack-tip region when the CTOA specimen was under load and when the crack was further extended, the casting was released.

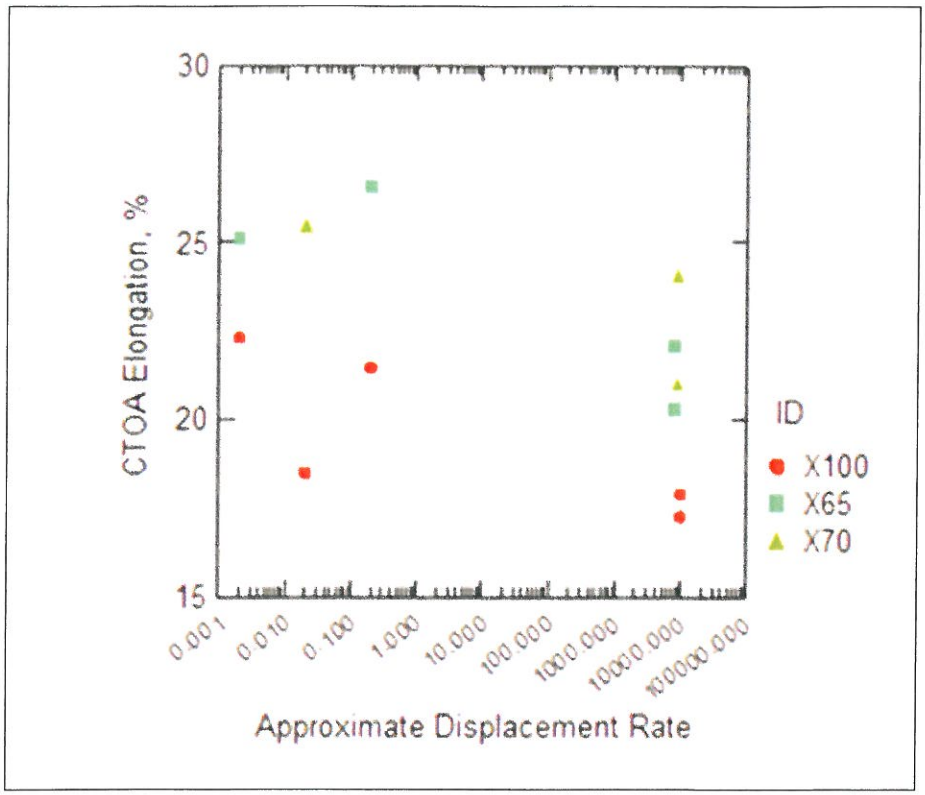

Fig.16. Changes in the elongation of the X-100, X-65, and X-70 steels with test rate.

something of a mixed mode, but is generally characterized as a slant fracture, because failure is essentially on a single shear plane, with no cup-cup or cup-cone shear region associated with the fracture. In addition, some regions along the full-scale tested pipe fractured in a pure slant mode, with little or no flat-fracture regions.

For the CTOA specimens, the slant-mode failures tend to have very little or no 'flat' fracture. The constraint differences and higher rate of crack growth in the full-scale pipe may have influenced the observed difference in fracture mode.

Differences in the appearance of the fracture surfaces from the full-scale test and laboratory CTOA tests are also apparent. No laboratory tests have produced fractures that reproduce all the features observed on the full-scale, high-rate test fractures. Interestingly, some of the quasi-static test fractures have more in common with appearance of the burst-test fracture than do the highest-speed CTOA fractures compared in this study. This is because a number of the X-100 tests conducted at 0.02 mm/s had intermittent crack growth, which has regions of dynamic crack growth that might be similar to the actual fracture conditions of the full-scale test.

Plastic deformation

Deformation through the gauge length of the reduced section indicates that the X-65 and X-70 steels are more ductile than the X-100 steel, with quasi-static values of around 25% while the X-100 has an elongation around 20%. As testing rates increase, the percent elongation decreases slightly for all three alloys (Fig.16). The results show that the deformation of the grid is in the loading direction and the grid rectangles rotate or deform in the cracking direction. The deformation of the grid lines shows non-uniform 'elongation' at the 'necked' regions.

Generally the X-100 and X-65 specimens show similar profiles for thinning due to plastic flow. The shoulder where the specimen thickness changes from 8 mm to 15 mm constrains the plastic flow, and thinning is limited in the first 6 mm or 7 mm from the shoulder, and then increases in a similar manner for all of the alloys and test rates evaluated. Both fracture modes follow the same basic trend, although the slant-shear fracture mode has less thinning during final fracture than the flat-fracture mode, which 'necks' during final fracture. The grids show little rotation, indicating that most of the plastic deformation is parallel to the load line.

Numerical modelling

The stable tearing behaviour of the CTOA test was modelled. Finite-element analysis (FEA) was applied to predict the applied load vs crack extension behaviour of steels #1 – #5, and showed correlation coefficients between the experimental and FEA results of between 0.92 and 0.993 [21]. This FEA model under-predicted the initial crack extension, when the crack extension was

less than twice the specimen thickness, and accurately described the crack extension behaviour beyond the peak stress. In another model, the focus was on X-100 steel, and the failure parameters of the Johnson-Cook and Hooputra *et al.* models were evaluated by parametrical computation [28]. From this work, the equivalent plastic-strain parameters of damage, for both the Johnson-Cook and Hooputra *et al.* models, were defined for X-100 steel.

A recent model also focused on X-100 steel [26] via the computational cell technique in simulation of slant-crack advance. The dependence of crack-growth parameters on the tilt angle was systematically investigated, and a simple GTN model was used to simulate ductile damage growth within the computational cells. The main results are summarized as follows:

- The energy dissipation rate R reaches a minimum value in the case of slant fracture for a final tilt angle equal to 45°. This result is consistently obtained for different material hardening or damage parameters. The energy dissipation rate correlates well with CTOA values.
- Stress and strain states in the stable tearing region hardly depend on the assumed tilt angle.
- The CTOA on the surface of the specimen is close to the CTOA at the centre of the specimen (steady-state propagation).

Future work

The difficulty in producing accurate and reproducible direct CTOA measurements on the surface of test specimens is clear from our results, and suggests the need for robust, automated measurement procedures and evaluation of indirect estimations of CTOA from load-displacement data. Furthermore, cross-head displacement has been used as a proxy for crack-mouth-opening displacement (CMOD), as the clip gauges typically used in these tests are prone to slip and lag behind when loading rates are increased. This indicates the need for improved dynamic displacement measurement which will require a novel test apparatus and specimen-preparation modifications, so that more-accurate correlations of crack location, velocity, crack-path, and crack morphology can lead to the understanding of the fracture mechanisms and their associated changes. Correlating crack-tip velocity to the applied load and far-field deformation for various pipeline steels, and methods of indirectly calculating CTOA, will likely be of interest for future FE-modelling efforts.

Acknowledgments

The authors thank the many guest researchers who were involved in developing and conducting CTOA tests over the years: P.P.Darcis, G.Kohn, A.Bussiba, A.Shtechman, R.Reuven, J.M.Treinen, and H.Windhoff.

References

1. A.B.Rothwell, 2000. Fracture propagation control for gas pipelines - past, present, and future. Pipeline Technology, 1. Elsevier, Netherlands, pp 387-405.
2. G.M.Wilkowski, Y.-Y.Wang, and D.L.Rudland, 2000. Recent efforts on characterizing propagating ductile fracture resistance of linepipe steels. Idem, pp 359-386.
3. S.H.Hashemi, I.C.Howard, J.R.Yates, R.M.Andrews, and A.M.Edwards, 2004. A single specimen CTOA test method for evaluating the crack tip opening angle in gas pipeline steels. Proc. International Pipeline Conference, pp 0610.1-7.
4. G.Demofonti, G.Mannucci, C.M.Spinelli, L.Barsanti, and H.-G.Hillenbrand, 2000. Large diameter X100 gas linepipes: fracture propagation evaluation by full-scale burst test. Pipeline Technology, 1. Elsevier, Netherlands, pp 509-520.
5. B.N.Leis, R.J.Eiber, L.Carlson, and A.Gilroy-Scott, 1998. Relationship between apparent (total) Charpy V-notch toughness and the corresponding dynamic crack propagation resistance. Proc. International Pipeline Conference, 2, pp 723-731.
6. J.C.Newman, Jr, and M.A.James, 2001. A review of the CTOA/CTOD fracture criterion - why it works! Proc. 42nd AIAA/ASME/ASCE/AH/ASC Structures, Structural Dynamics, and Materials Conference and Exhibit, paper AIAA-200-1324, Seattle, Washington, USA, pp 1042-1051.
7. N.Pussegoda, S.Verbit, A.Dinovitzer, W.Tyson, A.Glover, L.Collins, L.Carlson, and J.Beattie, 2000. Review of CTOA as a measure of ductile fracture toughness. Proc. International Pipeline Conference, 1. pp 247-254.
8. D.J.Horsley, 2003. Background to the use of CTOA for prediction of dynamic ductile fracture arrest in pipelines. *Eng Fract. Mech.* **70**, 3-4, pp 547-552.
9. G.Mannucci, G.Buzzichelli, P.Salvini, R.J.Eiber, and L.Carlson, 2000. Ductile fracture arrest assessment in a gas transmission pipeline using CTOA. Proc. International Pipeline Conference, 1, pp 315-320.
10. R.Jones and A.B.Rothwell, 1997. Alternatives to Charpy testing for specifying pipe toughness. Fracture control in gas pipelines. WTIA/APIA/CRC-MWJ International Seminar, pp 5-1-21.
11. O.E.O'Donoghue, M.F.Kanninen, C.P.Leung, G.Demofonti, and S.Venzi, 1997. The development and validation of a dynamic fracture propagation model for gas transmission pipelines. *Int. J.Pressure Vessels Piping*, 70, 1, pp 11-25.
12. N.Pussegoda, L.Malik, A.Dinovitzer, B.A.Graville, and A.B.Rothwell, 2000. An interim approach to determine dynamic ductile fracture resistance of modern high toughness pipeline steels. Proc. International Pipeline Conference, 1, pp 239-45.

13. R.M.Andrews, I.C.Howard, A.Shterenlikht,and J.R.Yates, 2002. The effective resistance of pipeline steels to running ductile fractures; modelling of laboratory test data. *In*: ECF14, Fracture mechanics beyond 2000. EMAS Publications, Sheffield, UK, pp 65-72.
14. D.S.Dawicke, 1996. Residual strength predictions using a CTOA criterion. Proc. FAA-NASA Symposium on Continued Airworthiness of Aircraft Structures, Atlanta, GA, USA.
15. K.-H.Schwalbe, J.C.Newman, Jr, and J.L.Shannon, Jr, 2005. Fracture mechanics testing on specimens with low constraint-standardisation activities within ISO and ASTM. *Eng Fract.Mech.*, **72**, pp 557-576.
16. ASTM ,2006. Standard E2472-06. Standard test method for determination of resistance to stable crack extension under low-constraint conditions. ASTM Book of Standards, West Conshohocken, PA, USA.
17. G.Demofonti, G. Buzzichelli, S.Venzi, and M.Kanninen, 1995. Step by step procedure for the two specimen CTOA test. Pipeline Technology, 2. Elsevier, Netherlands, pp 503-512.
18. A.Shterenlikht, S.H.Hashemi, I.C. Howard, J.R.Yates, and R.M.Andrews, 2004. A specimen for studying the resistance to ductile crack propagation in pipes. *Eng Fract. Mech.*, **71**, pp 1997-2013.
19. S.H.Hashemi, R.Gay, I.C.Howard, R.M.Andrews, and J.R.Yates, 2004. Development of a laboratory test technique for direct estimation of crack tip opening angle. Proc. 15th European Conference of Fracture, Stockholm, Sweden.
20. S.H.Hashemi, I.CHoward, J.R.Yates, R.M.Andrews, and A.M.Edwards, 2004. Experimental study of thickness and fatigue precracking influence on the CTOA toughness values of high grade gas pipeline steel. Proc. International Pipeline Conference, pp 0681.1-8.
21. P.P.Darcis, G.Kohn, A.Bussiba, J.D.McColskey, C.N.McCowan, R.Fields, R.Smith, and J.Merritt, 2006. Crack tip opening angle: measurement and modeling of fracture resistance in low and high strength pipeline steels. Idem, IPC2006-10172.
22. A. Shtechman, C.N.McCowan, R.Reuven, E.Drexler, Ph.Darcis, J.M.Treinen, R.Smith, J.Merritt, T.A.Siewert, and J.D.McColskey, 2008. Dynamic apparatus for the CTOA measurement in pipeline steels. Idem, IPC2008-64362.
23. P.P.Darcis, C.N.McCowan, H.Windhoff, J.D.McColskey, and T.A.Siewert, 2008. Crack tip opening angle optical measurement methods in five pipeline steels. *Eng Fract. Mech.*, **75**, pp 245-246.
24. R.Reuven, E.Drexler, C.McCowan, A.Shtechman, P.Darcis, M.Treinen, R.Smith, J.Merritt, T.A.Siewert, and J.D.McColskey, 2008. CTOA results for X65 and X100 pipeline steels: influence of displacement rate. Proc. International Pipeline Conference, IPC2008-64363.
25. S.Xu, W.R.Tyson, R.Eagleson, C.N.McCowan, E.S.Drexler, J.D.McColskey, and PhP Dacis, 2010. Measurement of CTOA using MDCB and DWTT specimens. Idem, IPC2010-31076.
26. J.Besson, C.N.McCowan, and E.S.Drexler, 2013. Modeling flat to slant fracture transition using the computational cell methodology. *Eng Fract. Mech.*, **104**, pp 80-95.
27. J.W.Sowards, C.N.McCowan, and E.S.Drexler, 2012. Interpretation and significance of reverse chevron-shaped markings on fracture surfaces of API X100 pipeline steels. *Mat. Sci. Eng A – Struct.*, **551**, pp 140-148.
28. M.Szanto, C.N.McCowan, E.S.Drexler, and J.D.McColskey, 2011. Fracture of X100 pipeline steel: combined experimental-numerical process. NIST BERB publication (B2011-0116).
29. R.J.Fields, J.D.McColskey, C.N.McCowan, P.P.Darcis, E.S.Drexler, S.P.Mates, and T.A.Siewert, 2012. Mechanical properties and crack behavior in line pipe steel. Final Report to the Department of Transportation. http://primis.phmsa.dot.gov/matrix/FilGet.rdm?fil=7883.
30. E.S.Drexler, PhP.Darcis, C.N.McCowan, J.W.Sowards, J.D.McColskey, and T.A.Siewert ,2011. Ductile-fracture resistance in X100 pipeline welds measured with CTOA. *Weld J.*, **90**, 12, pp 241-s - 248-s.
31. PhP.Darcis, C.N.McCowan, J.D.McColskey, and R.Fields, 2008. Crack tip opening angle measurement through a girth weld in an X100 steel pipelines. *Fatigue Fract. Mater. Struct.*. **31**, pp 1065-1078.
32. ASTM, 1999. Standard E1290-99. Standard test method for crack tip opening displacement (CTOD) fracture toughness measurement. ASTM Book of Standards, West Conshohocken, PA, USA.
33. K.-H.Schwalbe, J.C.Newman, Jr, and J.L.Shannon, Jr, 2005. Fracture mechanics testing on specimens with low constraint-standardisation activities within ISO and ASTM. *Eng Fract. Mech.*, **72**, pp 557-576.
34. K.-H.Schwalbe, J.Heerens, U.Zerbst, H.Pisarski, and M.Kocak, 2002. EFAM-GTP 02, The GKSS test procedure for determining the fracture behaviour of materials, 2nd issue. GKSS Report 2002/24, GKSS-Forschungszentrum Geesthacht.
35. ISO/FDIS 22889, 2013. Metallic materials: method of test for the determination of resistance to stable crack extension using specimens of low constraint.
36. J.Heerens and M.Schodel, 2003. On the determination of crack tip opening angle, CTOA, using light microscopy and delta-5 measurement technique. *Eng Fract. Mech.*, **70**, 3-4, pp 417-426.
37. S.H.Hashemi, 2012. Comparative study of fracture appearance in crack tip opening angle testing of gas pipeline steels. *Mat. Sci. Eng A – Struct.*, **558**, pp 702-715.